The medium coupling effect on propagation of guided waves in engineering structures and human bone phantoms

Jiangang Chen[1], Zhongqing Su*[2] and Li Cheng[2]

[1]*Department of Biomedical Engineering, Columbia University, New York, NY, The USA*
[2]*Department of Mechanical Engineering, The Hong Kong Polytechnic University, Kowloon, Hong Kong*

Abstract. As a result of the medium coupling, propagation characteristics of ultrasonic waves guided by a multi-phase medium can be different from those in a homogeneous system. This phenomenon becomes prominent for a medium consisting of phases with considerably distinct material and physical properties (e.g., submerged structures or human bones covered with soft tissues). In this study, the coupling effect arising from both fluid and soft tissues on wave propagation in engineering structures and human bone phantoms, respectively, was explored and calibrated quantitatively, with a purpose of enhancing the precision of ultrasonic-wave-based non-destructive evaluation (NDE) and clinical quantitative ultrasound (QUS). Calibration results were used to rectify conventional NDE during evaluation of corrosion in a submerged aluminium plate, and QUS during prediction of simulated healing status of a mimicked bone fracture. The results demonstrated that with the coupling effect being appropriately taken into account, the precision of NDE and QUS could be improved.

Keywords: medium coupling; guided waves; non-destructive evaluation; quantitative ultrasound

1. Introduction

Propagation of elastic waves in the media comprising multiple phases is of a great interest in the engineering practice. As a consequence of the medium coupling effect, elastic waves can be modulated, to different extents for different wave modes, presenting many somewhat subtle traits and behaving differently from their counterparts in a medium of a single phase. Most existing elastic-wave-based NDE techniques have been well-developed for materials or structures of a single component (e.g., homogeneous alloys) or multiple but similar components (composite laminates) in a free status (Lee *et al*. 2010, Lu *et al*. 2010, Yu and Ma 2012). When applied to objects with coupled media (such as a boat hull, pillar of offshore platform or petroleum pipeline (solids) submerged in seawater (fluid) (Na and Kundu 2002), the coupling effect can prevent these NDE techniques from delivering precise results. To calibrate and rectify the influence of medium coupling on wave propagation, in particular when the coupled medium has very distinct properties from the one principally accommodating wave propagation (e.g., one being relatively 'soft' such as fluid or soft

tissue, while the other relatively 'hard' such as alloy or cortical bone), remains relevant but challenging.

The coupling effect from fluid on elastic waves in plate/shell-like structures has been drawing attentions over the years (in these cases the elastic waves take the form of Lamb waves). Yapura and Kinra (1995) analytically studied the propagation of Lamb waves in a fluid-solid coupled bi-layer system, to show that the surrounding fluid could alter the properties of Lamb waves. This conclusion was experimentally validated by Moilanen *et al.* (2006). On the other hand, Lamb waves in thin-walled tubular structures were explored by Cheeke *et al.* (1998, 1999), to capture a decrease in the velocity when the tube was filled with fluid. All these studies have reach some important conclusions regarding the medium coupling effect on wave propagation, whereas hitherto there is a lack in quantitative compensation for such a coupling effect for practical implementation of ultrasonic-wave-based NDE.

The above concern also exists in biomedical ultrasound applications. In clinical quantitative ultrasound (QUS), apart from the degenerative disorders of bone, the coupled soft tissues (skin, muscle, marrow, *etc.*) can also modulate ultrasound waves propagating in bone (Moilanen *et al.* 2006, 2008, Chen *et al.* 2010a, 2012a,b). This effect is often ignored in clinical practice, and implementation of QUS is simply based on the simplified theorem of elastic waves in single-medium solids in a free status, leading to less precise assessment without differentiating the influence of coupled soft tissues from that due to the degradation in bone.

It is the abovementioned deficiencies in the current endeavours to develop ultrasonic wave-based NDE for engineering structures and QUS for bone assessment that have motivated the present work. The coupling effect from fluid and soft tissue mimicking on ultrasonic waves were investigated and calibrated quantitatively, via a three-dimensional (3D) finite element (FE) analysis and a testing approach. Calibration results were employed to rectify traditional NDE during detecting corrosion in a submerged aluminium plate and QUS during predicting the healing progress of mimicked bone fracture.

2. Waves in coupled medium

In a medium comprising multi-phases (e.g., a plate submerged in liquid or a pipe buried in soil, the human bone covered with a layer of soft tissue), the coupling between two phases introduces confinements to the particulate motion at the interface, and provides a radiation way for Lamb waves in the plate to leak into the coupled medium, referred to as *leaky Lamb waves*. Under this coupling effect, Lamb waves in a multi-phase medium behave differently from those in a free plate, and moreover the influence can be distinct for different modes. In particular for an fluid-solid coupled medium of an infinite in-plane dimension (fluid thickness: a, half plate thickness: h), the characteristic equation for this two-phase medium can be described, if both the solid and fluid deemed isotropic and the latter is unable to sustain shear loads, as (Moilanen *et al.* 2006)

$$det(G(\omega, k, a, h, \rho, \rho_F, c_F, c_L, c_T)) = 0 \qquad (1)$$

Where G is the characteristic matrix, ω the circular frequency, k the wavenumber, a and h the thickness of the coupled fluid layer and half thickness of the solid layer, respectively; ρ and ρ_F the density of the solid layer and coupled fluid layer, respectively; c_F the bulk wave velocity in the fluid

layer; c_L and c_T the velocity of the longitudinal and transverse (shear) wave mode in the plate, respectively. Solutions to Eq. (1) depict dispersion properties of Lamb waves in this two-phase medium (Moilanen *et al.* 2006).

3. Methodology

Consider two scenarios: (i) an aluminium plate ($600 \times 600 \times 1.6$ mm^3) coupled with a layer of water, both having the same in-plane dimension but the thickness of latter varied from 0 to 10 mm with an increment of 1 mm; and (ii) a soft tissue-bone phantom that is comprised of a bone-mimic phase (using acrylic materials) ($460 \times 240 \times 2$ mm^3) and a soft tissue-mimic phase (using artificial silicon rubber (ASR)) with variance in thickness (i.e., 0.8, 1.9, 3.4, 4.2, 5.1, 6.3, 7.7, 9.4 mm). The two phases have the same in-plane dimension and are tied through an interface. In what follows, both the aluminium and acrylic are called the *hard phase*, while water and ASR the *soft phase*. The coupling effect was ultrasonically investigated for the above mentioned two scenarios, via 3D FE analysis and experimental testing.

3.1 3D FE modelling and simulation technique

In FE modelling, the hard phase was modelled using 3D eight-node brick elements, while soft phase was modelled either using 3D eight-node acoustic elements (for water) or using 3D eight-node brick elements (for ASR). A transducer pair (a transmitter and a receiver) was placed in tandem at the interface of two phases, as shown schematically in Fig. 1(a), to activate and receive ultrasonic waves in terms of axial transmission measurement. Note that, aimed at exploring the medium coupling effect on waves in bone, the transducer pair was positioned at the interface between two phases rather than atop the soft phase. The interface between the hard and soft phases was modelled using a specialised surface-based coupling constraint in virtue of a node-to-surface formulation, which is provided by ABAQUS®/EXPLICIT and therein named '*TIE*'. The transmitter and receiver were modelled using a piezoelectric model (Su and Ye 2009). Dynamic FE simulation was accomplished using ABAQUS®/EXPLICIT.
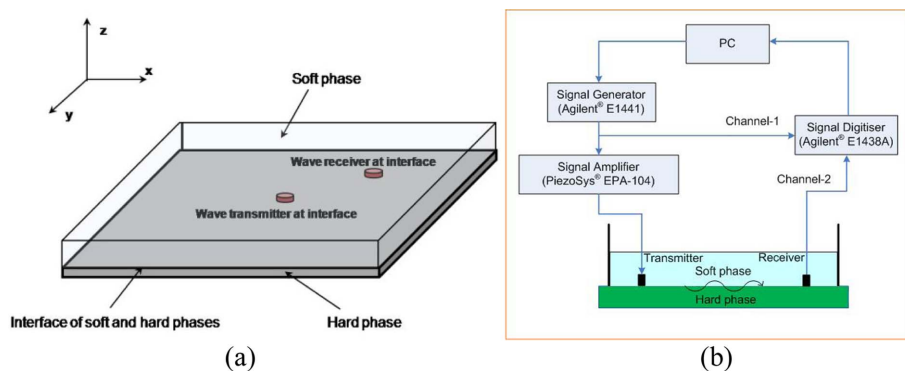

Fig. 1 (a) Allocation of transmitter and receiver at the interface between soft and hard phases and (b) configuration of experimental setup for *in vitro* testing

3.2 Testing approach

An *in vitro* testing approach including supporting software/hardware for implementation was developed. A pair of water-proof ultrasound transducers (Panametrics-V303-SU, central frequency: 1 MHz, nominal diameter: 13 mm), serving as the wave transmitter and receiver, respectively, was instrumented with a signal generation and data acquisition system configured on a *VXI* platform (Su and Ye 2009), as shown in Fig. 1(b). The transducer pair was collocated at the interface of two phases. With the system, diagnostic signals, i.e., five-cycle *Hanning*-windowed sinusoid tonebursts, were first customised in MATLAB® and downloaded to an arbitrary waveform generation unit (Agilent® E1441), in which D/A conversion was performed. The analog signals were amplified to 180 V (peak-to-peak) with a linear amplifier (PiezoSys® EPA-104) to drive the transmitter. Wave signals were captured with the receiver through a signal digitiser (Agilent® E1438A) at a sampling rate of 25 MHz. Phantoms were supported on all their edges on an optical testing table (NEWPORT® ST-UT2).

4. Results and discussion

4.1 Coupling effect arising from fluid

The coupling effect arising from fluid was first investigated by ultrasonically interrogating an aluminium plate whose upper surface was in contact with a layer of pure water (the thickness of the water layer varied from 0 to 10 mm with an increment of 1 mm), via 3D FE modelling and simulation (Section 3.1) and experiment (Section 3.2). The Hilbert transform (HT)-processed signals captured under the optimised excitation at 150 kHz, when the soft phase was 5 mm in thickness as a representative case, is displayed in Fig. 2(a). For comparison, signals captured in the same hard phase but in the absence of the soft phase are included in the figures. The coupled soft phase exerts strong influence on characteristics of the A_0 mode, manifesting as twofold: (i) a reduction in the signal/energy magnitude; and (ii) a delay in the arrival time as a result of reduced propagation velocity. However it does not modulate S_0 to a perceptible level.
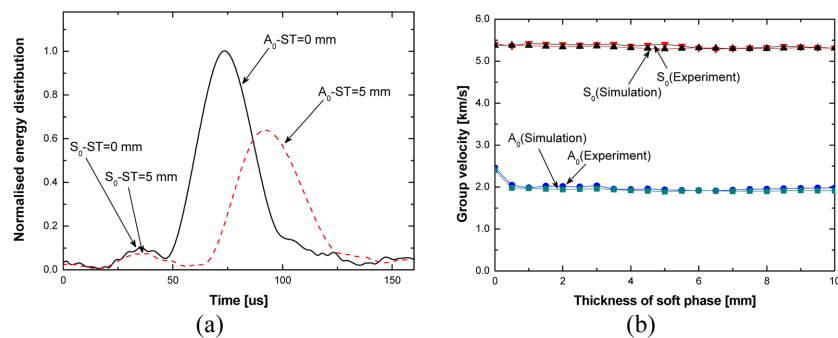

Fig. 2 (a) HT-processed results of signals in an aluminium plate in the absence (ST = 0) and presence of a layer of pure water (ST = 5 mm) at excitation frequencies of 150 kHz (ST: thickness of soft phase) and (b) group velocities of S_0 and A_0 in an aluminium plate obtained through simulation and *in vitro* testing *vs*. thickness of the coupled pure water layer (excitation frequency: 150 kHz)
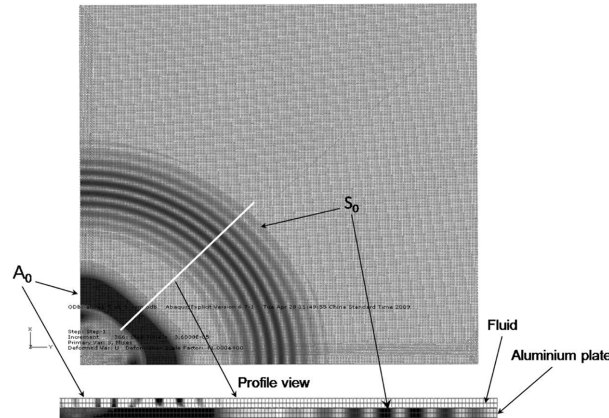
Fig. 3 Schematic illustration of stress distribution during wave propagation in fluid-solid coupled medium, showing energy leakage of the A_0 mode (for comparison, displayed stress distribution in the fluid layer and in aluminium plate is not of the same scale; the darker the greyscale the higher the stress is)
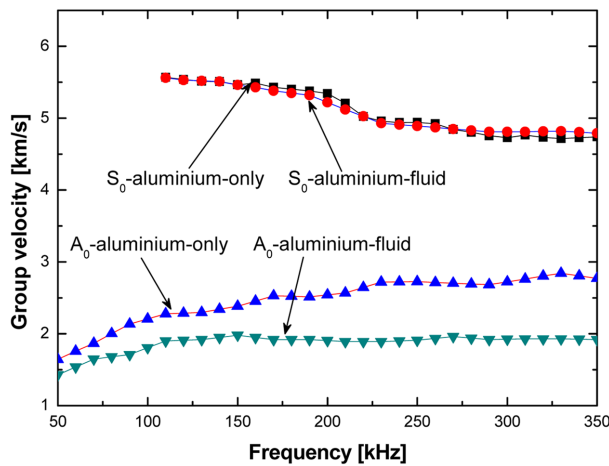

Fig. 4 Dispersion curves of Lamb waves in an aluminium plate in the absence and presence of a fluid layer (4 mm in thickness) obtained via FE simulation and experiment

Fig. 2(b) shows velocities of two concerned wave modes, subject to thickness of the coupled soft phase, recapitulating that the coupled soft phase exerts strong influence on characteristics of the A_0 mode. However it does not modulate S_0 to a perceptible level. They also highlight that the most significant changes of A_0 occur when the soft phase is initially introduced, and as the thickness of the soft phase increases, further influence from the soft phase is mild.

To strengthen this interpretation, the stress field across the thickness of this two-phase system as a result of wave propagation (when the soft phase is 5 mm thick) was obtained, shown in Fig. 3, to observe that partial energy associated with A_0 leaks out from the hard to the soft phase, but energy associated with S_0 is confined in the hard phase.

Further, the above examination was extended to a sweep frequency range from 50 to 350 kHz. The result is shown in Fig. 4, based on which, influence of the fluid coupling on A_0 was quantitatively calibrated, subjected to the thickness of the fluid layer.

4.2 Coupling effect arising from soft tissues

Layers of ASR with different thicknesses but the same elastic properties (E_{ASR} = 11.96 *kPa*) were explored at the frequency of 75 kHz. As some representative results, HT-processed signals when the thickness of ASR layer is 0.8, 3.4, 4.2, 7.7 and 9.4 mm, respectively, are combined in Fig. 5. Further, including all the discussed thicknesses of the soft phase (0.8~9.4 mm), changes in velocities of S_0 and A_0, and changes in their peak energy magnitudes, subject to thickness of the coupled ASR layer, are summarised in Figs. 6(a) and (b), respectively. Figs. 5 and 6 highlight observations that the coupled ASR layer exerts influence on both S_0 and A_0 obviously, reducing signal magnitudes and decreasing velocities, for both whereas at different degrees. The most significant changes take place when the ASR layer is initially introduced, and decrease in signal magnitude continues as ASR thickness increases, but propagation velocities of both modes fluctuate very slightly with further increase of ASR thickness. It is different from the case when a pure fluid layer serving as the soft
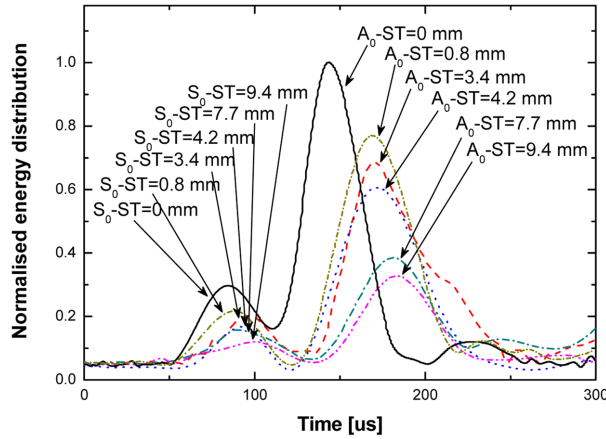

Fig. 5 HT-processed results of signals experimentally captured from phantoms in the absence and presence of a layer of ASR of different thickness (excitation frequency: 75 kHz; ST: thickness of soft phase (ASR); signal being normalised relative to the amplitude extremum of the signal in the absence of ASR)
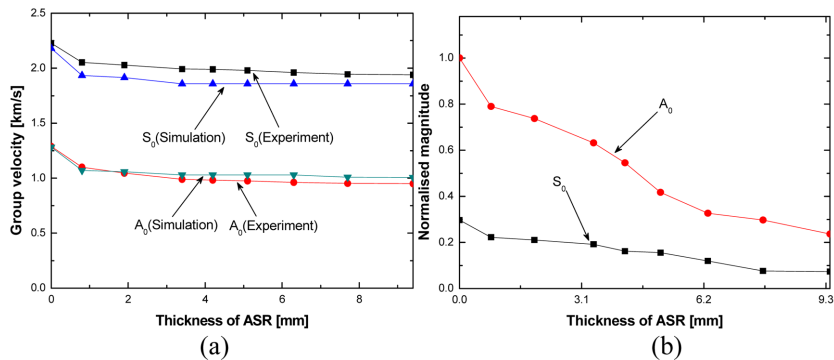

Fig. 6 (a) Group velocities and (b) magnitudes of S_0 and A_0 in bone phantoms (ASR thickness from 0.8 to 9.4 mm) vs. thickness of the coupled ASR layer (signal magnitude being normalised relative to the amplitude extremum of the signal in the absence of ASR)
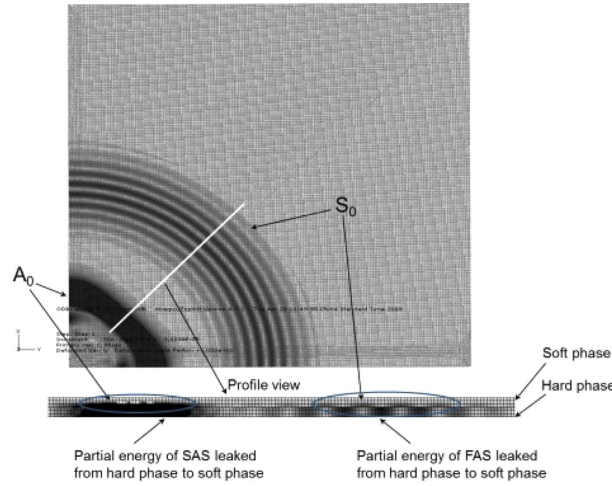
Fig. 7 Stress field of wave in bone phantom coupled with a layer of ASR (3.4 mm in thickness), showing that energies associated with both S_0 and A_0 leak from hard to soft phase (note: for convenience of comparison, the displayed stress fields in the hard and soft phases are not of the same scale; the darker the greyscale the higher the stress is)
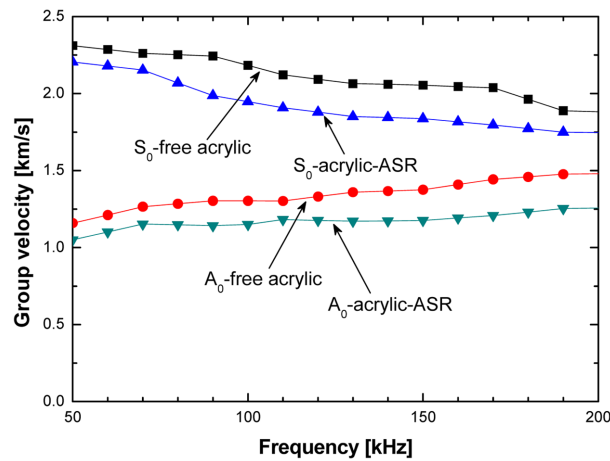

Fig. 8 Dispersion curves of S_0 and A_0 in bone phantoms without and with a layer of ASR (3.4 mm in thickness)

phase (Section 4.1) in which prominent modulation on ultrasonic waves due to existence of the coupled medium can be noticed for A_0 only.

To visualise the wave leakage from the hard to soft phase, the stress field throughout thickness of the two-phase phantom (ASR thickness: 3.4 mm) is shown in Fig. 7, to see prominent leakage of energy from the hard to soft phase for both modes. It implies that, because soft tissues support both in-plane (longitudinal and SH wave modes) and out-of-plane (SV mode) particulate motion patterns, soft tissues provide a radiation way for S_0 and A_0 to leak into overlying soft tissues.

To study the dispersion property of the discussed waves, S_0 and A_0 were activated in a sweep frequency range from 50 to 200 kHz. The obtained dispersion curves of two modes in the absence and presence of a soft phase (a layer of ASR 3.4 mm in thickness) is plotted in Fig. 8. Results

reiterate that the coupling effect of soft phase on S_0 and A_0 exists across the whole discussed frequency range: ASR exerts strong coupling influence on both wave modes, exhibiting as reduced propagation velocities.

Throughout the study the most prominent modulations from a coupled soft phase on propagation velocities of S_0 and A_0 take place when the soft phase is initially introduced, and there is no phenomenal discrepancy in such a modulation when the soft phase has different thicknesses (Figs. 5 and 6(a)). This implies that the surrounding soft tissues exert perceptible influence on the speed of ultrasonic Lamb waves only in a confined area, making it possible to extend the compensation for such an influence at a specific thickness of the soft phase to general cases, if only the velocity concerned in bone assessment. Nevertheless, a continuous and increasing modulation on signal magnitude can be seen with an increase in thickness of ASR (Fig. 6(b)). It articulates that rectification for such a coupling effect is case-dependent and compensation should be applied according to the calibrated relationships between changes in signal magnitude and changes in soft phase (Fig. 6(b)) if signal magnitude is also a factor in bone assessment.

5. Applications

5.1 Application to NDE for corrosion detection of submerged structures

In this section, the calibrated influence of fluid coupling on Lamb wave propagation (Section 4.1) was applied to the evaluation of corrosion damage (15 mm in diameter and 1 mm in depth) in a submerged aluminium plate (600 mm × 600 mm × 1.6 mm) using the probability-based diagnostic imaging (Chen *et al.* 2010b). The upper surface of the aluminium plate was in contact with a fluid layer of varying thicknesses. A pair of water-proof immersion transducers, the same as that described in Section 3.2, was employed to perform a pulse-echo measurement at different positions at the interface of the fluid layer and aluminium plate, offering three sensing paths, T_1-R_1, T_2-R_2 and T_3-R_3 (Fig. 9(a)). Signal generation/acquisition was accomplished with the system developed on a *VXI* platform (Fig. 1(b)). Five-cycle *Hanning*-windowed sinusoid tonebursts at a central frequency of 150 kHz were excited and applied to the transmitter at three positions (Fig. 9(a)) in turn after
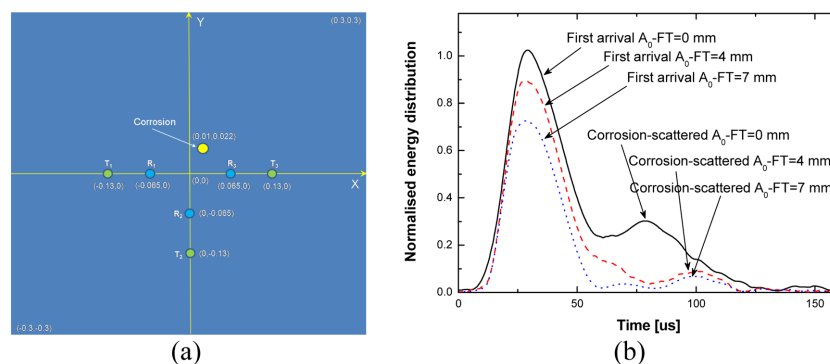

Fig. 9 (a) An aluminium plate containing corrosion damage (unit: m) and (b) HT-processed wave signals captured via sensing path T_3-R_3 in the aluminium plate containing corrosion damage in the absence and presence of fluid layers of different thicknesses, obtained via experiment (FT: fluid layer thickness)
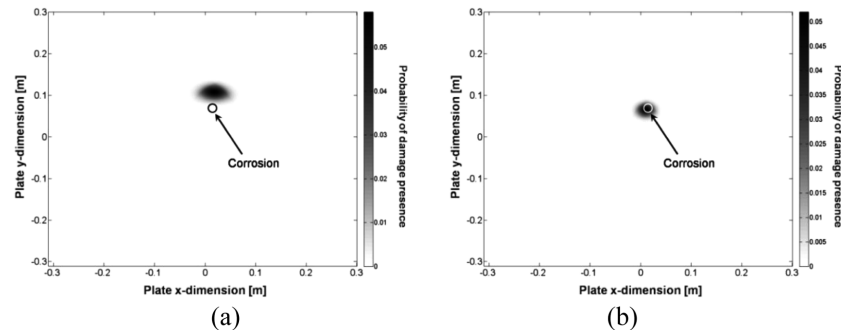
Fig. 10 Identification results of corrosion damage in the aluminium plate coupled with fluid layer of different thicknesses: (a) without rectification and (b) with compensation for the coupling effect (the fluid layer is 4 mm in thickness) (white or black circle: actual corrosion)

amplified to 180 V_{p-p}. The Lamb wave signals were captured via three sensing paths at a sampling rate of 25 MHz.

Fig. 9(b) shows the HT -processed signals experimentally captured via sensing path T_3-R_3, as example, in the absence and presence of fluid layers of different thicknesses (4 and 7 mm, respectively). Following steps of the probability-based diagnostic imaging, each sensing path contributed to a probability image. Upon fusion of images, the identified results are shown in Fig. 10, without (Fig. 10(a)) and with (Fig. 10(b)) the rectification and compensation for the fluid coupling influence on Lamb wave propagation. Using the rectified wave propagation velocity by compensating for the fluid coupling, it can be seen that the identification results of corrosion damage in the submerged aluminium plate are satisfactory. For the sake of brevity, only the results obtained via experiment (fluid thickness being 4 mm) were presented in Fig. 10, although good agreement between FE simulation and experiment was achieved.

5.2 Application to monitoring of mimicked healing progress of fractured bone

When QUS is conducted *in vivo*, the coupling effect of soft tissues on S_0 and A_0 cannot be avoided, which is, however, sometimes neglected in the clinical practice, leading to compromised prediction accuracy. In the following, as an application of the results arising from the above study, the coupling effect of soft tissues on A_0 was compensated, so as to improve the accuracy of A_0-based QUS when used for predicting a certain healing status of mimicked bone fracture. To simulate a fractured bone at different healing statuses, a series of samples was fabricated in accordance with the following procedures: two identical acrylic plates (230 mm × 240 mm × 3.2 mm each) were connected via an ASR strip (Young's modulus being 2.8 MPa, close to that of the callus in a real fractured bone at its early healing stage (Protopappas *et al.* 2007)), as sketched in Fig. 11(a). At different healing stages, calluses are of different sizes and elastic properties, and therefore their geometric features can be used to indicate the healing progress of bone fracture. Seven such samples were made, each having an ASR strip of different width (along the axial direction of the sample), from 0 to 6 mm with an increment of 1 mm. These seven samples imitated a fractured bone at seven healing statuses (0 mm standing for a healthy bone). Five-cycle *Hanning*-window modulated sinusoidal tonebursts at 100 kHz were used as the diagnostic signal. Correlation between the reduction rate in the propagation velocity of A_0 and width of callus was obtained, in Fig. 12(a), which was used to determine the bone healing progress.
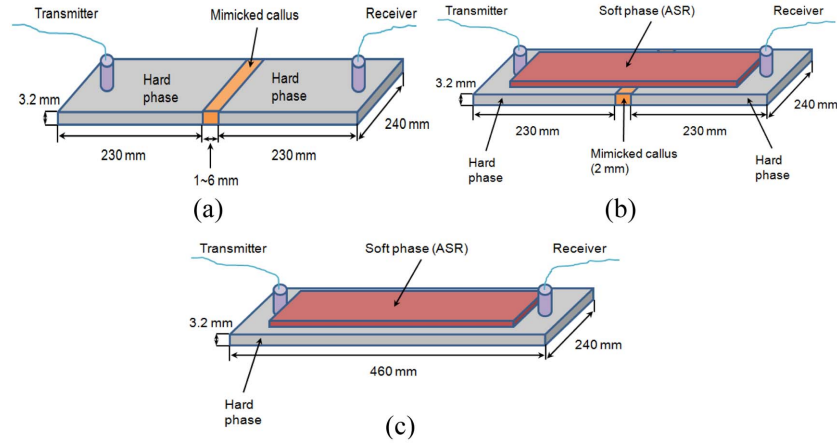
Fig. 11 Schematic of bone samples with mimicked callus for imitating bone fracture: (a) without coupled ASR layer, (b) with coupled ASR layer when callus is 2 mm wide and (c) with coupled ASR layer but without any mimicked callus (healthy bone sample)
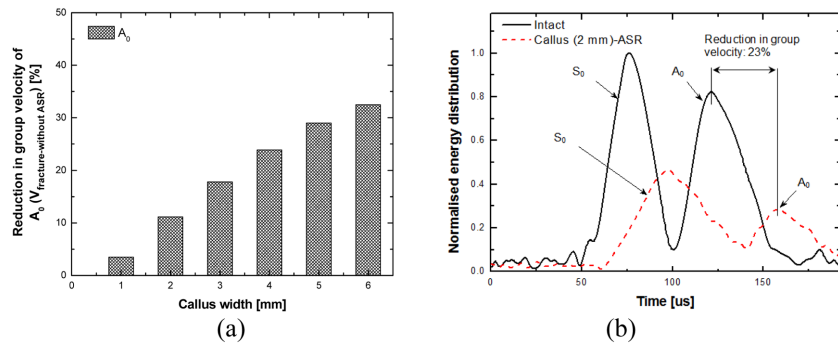

Fig. 12 (a) Reduction in propagation velocity of A_0 vs. width of callus (reflecting different healing stages) (note: correlation in this figure was established in the absence of overlying soft tissues) and (b) HT-processed results of signals experimentally captured from intact sample (containing neither callus nor coupled overlying soft tissues) and mimicked fractured bone sample (with both callus and coupled overlying soft tissues)

Note that the velocity of A_0 shown in Fig. 12(a) was measured from the fractured bone sample without any coupled soft tissues (Fig. 11(a)), and it is denoted by $V_{fracture-without\ ASR}$.

To introduce the coupling effect of soft tissues, a layer of ASR (160 mm × 60 mm × 3.4 mm, $E_{ASR} = 11.96\ kPa$) was adhered to one of the above seven samples (with a callus width of 2 mm), serving as the overlying soft tissues, as elucidated in Fig. 11(b). A transducer pair was positioned at the interface between the hard and soft phases, clamping the soft phase in the axial direction (see Fig. 11(b)). Note that as iterated earlier, aimed at exploring the coupling effect of the soft medium on waves propagating in the hard phase, the transducer pair was positioned at the interface rather than atop the soft phase, which is different from real clinical applications of QUS. Signals captured from samples with such a configuration (with both callus and coupled soft tissues) could be deemed as *in vitro* signals in a fractured bone, and the velocity of A_0 accordingly determined from these signals is denoted by $V_{fracture-with\ ASR\ (in\ vitro)}$ in what follows.

In the following, A_0-based QUS was used to predict the current callus width (2 mm), without and with compensation for the coupling effect from the overlying ASR.

5.2.1 Without compensation for coupling effect

In the test, the relative reduction rate in the velocity of A_0 in the sample sketched in Fig. 11(b) (with callus of 2 mm and coupled ASR layer, i.e., $V_{fracture\text{-}with\ ASR\ (in\ vitro)}$) with regard to the velocity of A_0 in an intact bone sample (containing neither callus nor coupled ASR layer, Fig. 11(a), denoted by $V_{no\ fracture\text{-}without\ ASR}$), $R_{in\ vitro\text{-}intact}$ (i.e., $R_{in\ vitro\text{-}intact} = (V_{no\ fracture\text{-}without\ ASR} - V_{fracture\text{-}with\ ASR\ (in\ vitro)}) /$ $V_{no\ fracture\text{-}without\ ASR}$), was determined to be 23% from the captured signals, as shown in Fig. 12(b). Without consideration of coupling effect, such a reduction was fully attributed to the existence of callus. Based on the relationship between velocity reduction in A_0 and callus width (Fig. 12(a)), callus in the current healing status was predicted to be 4 mm in width, largely deviated from the actual callus width of 2 mm.

5.2.2 With compensation for coupling effect

Conclusions obtained from previous parametric studies indicate that, apart from degradation in bone including callus, the coupling effect of overlying soft tissues also causes reduction in the velocity of A_0. Such an effect should be appropriately removed before using Fig. 12(a) to predict the callus width, because the correlation in Fig. 12(a) was established in the absence of any overlying soft tissue.

Because the callus width was much smaller than the axial dimension of the fractured bone sample, waves propagating within callus along its width would not be affected by the surrounding soft tissues. This means that the overall influence of coupled soft tissues on waves propagating in the entire fractured bone (with coupled ASR layer and callus) can be hypothesised to be the same as that in a healthy bone (with the same coupled ASR layer but without any callus, shown in Fig. 11(c)), namely

$$\frac{V_{fracture-without\ ASR} - V_{fracture-with\ ASR\ (in\ vitro)}}{V_{fracture-without\ ASR}} = \frac{V_{no\ fracture-without\ ASR} - V_{no\ fracture-with\ ASR}}{V_{no\ fracture-without\ ASR}} \quad (2)$$

where $V_{no\ fracture\text{-}with\ ASR}$ is the velocity of A_0 in the sample shown in Fig. 11(c). The right term of Eq. (2), $(V_{no\ fracture\text{-}without\ ASR} - V_{no\ fracture\text{-}with\ ASR}) / V_{no\ fracture\text{-}without\ ASR}$ indicates the reduction rate in the velocity of A_0, fully due to the coupling effect of ASR layer, propagating in a healthy bone without fracture, therefore denoted by $R_{coupling}$ (i.e., $R_{coupling} = (V_{no\ fracture\text{-}without\ ASR} - V_{no\ fracture\text{-}with\ ASR}) / V_{no\ fracture\text{-}without\ ASR}$). Then we have

$$\frac{V_{fracture-without\ ASR} - V_{fracture-with\ ASR\ (in\ vitro)}}{V_{fracture-without\ ASR}} = R_{coupling} \quad (3)$$

On the other hand, referencing the calibrated coupling effect of ASR on A_0 as shown in Fig. 8, which was obtained using the same sample as that in Fig. 11(c), $R_{coupling}$ was determined to be 12% at the current excitation frequency of 100 kHz (i.e., $(V_{fracture\text{-}without\ ASR} - V_{fracture\text{-}with\ ASR\ (in\ vitro)}) / V_{fracture\text{-}without\ ASR}$ $= R_{coupling} = 12\%$). In addition, with knowing

$$R_{in\ vitro-intact} = \frac{V_{no\ fracture-without\ ASR} - V_{fracture-with\ ASR\ (in\ vitro)}}{V_{no\ fracture-without\ ASR}} \quad (4)$$

we have

$$\frac{V_{no\ fracture-without\ ASR} - V_{fracture-without\ ASR}}{V_{no\ fracture-without\ ASR}} = \frac{R_{in\ vitro-intact} - R_{coupling}}{1 - R_{coupling}} \qquad (5)$$

Observing the subscript of all variables in the left term of Eq. (5), it can be seen that this defined reduction in the velocity of A_0 had been compensated by considering the coupling effect from soft tissues, which can be now directly used to predict the callus width in terms of Fig. 12(a). Substituting the measured relative reduction rates ($R_{in\ vitro\text{-}intact} = 23\%$ and $R_{coupling} = 12\%$) from captured signals into Eq. (5), it has

$$\frac{V_{no\ fracture-without\ ASR} - V_{fracture-without\ ASR}}{V_{no\ fracture-without\ ASR}} = \frac{R_{in\ vitro-intact} - R_{coupling}}{1 - R_{coupling}} = \frac{23\% - 12\%}{1 - 12\%} = 12.5\% \qquad (6)$$

Using the reduction in velocity of A_0 of 12.5% rather than 23% (used in Section 5.2.1), the predicted callus width is circa 2 mm, tallying with the real callus width.

6. Conclusions

The effect of coupled medium (e.g., fluid or soft tissue) on Lamb wave propagation in engineering structures and human bones can pose great challenge on NDE and QUS techniques for delivering high precision evaluation. The investigation on such a coupling effect, conducted in this study, demonstrated that the S_0 and A_0 are sensitive to the coupling medium, manifested as reduced propagation velocity and signal magnitude as a result of the coupling. The alteration in the wave propagation resulted in impaired precision and accuracy of either NDE for corrosion in submerged structures or QUS for monitoring the healing progress of bone fracture. However, with consideration of and compensation for such a coupling effect, the precision and accuracy of both applications (NDE and QUS) were significantly improved, leading to precise prediction of the location of the corrosion and accurate determination of the current bone healing stage. This study recapitulates that coupling effect due to fluid/soft tissue on ultrasonic waves should be quantitatively taken into account when developing high-precision NDE and QUS techniques.

References

Cheeke, J.D.N., Li, X. and Wang, Z. (1998), "Observation of flexural Lamb waves (A0 mode) on water-filled cylindrical shells", *J. Acoust. Soc. Am.*, **104**(6), 3678-3680.

Cheeke, J.D.N., Shannon, K. and Wang, Z. (1999), "Loading effects on A0 Lamb-like waves in full and partially filled thin-walled tubes", *Sensor. Actuat. B. - Chem.*, **59**(2-3), 180-183.

Chen, J., Su, Z. and Cheng, L. (2010a), "Influence of soft tissues on propagation of ultrasonic Lamb waves in synthesised soft tissue-bone phantoms", *IFMBE Proceedings*, **31**(6), 1315-1318.

Chen, J., Su, Z. and Cheng, L. (2010b), "Identification of corrosion damage in submerged structures using fundamental anti-symmetric Lamb waves", *Smart Mater. Struct.*, **19**(1), 015004.

Chen, J., Foiret, J., Minonzio, J.G., Talmant, M., Su, Z., Cheng, L. and Laugier, P. (2012a), "Measurement of guided mode wavenumbers in soft tissue-bone mimicking phantoms using ultrasonic axial transmission", *Phys.*

Med. Biol., **57**(10), 3025-3037.

Chen, J., Su, Z. and Cheng, L. (2012b), "The effect of soft tissue coupling on propagation characteristics of ultrasonic waves: Calibration and application to quantitative ultrasound (QUS)", *Ultrasonics*, (In press).

Lee, J., Na, W.B. and Kim, J.T. (2010), "Curvature effect on Guided Wave propagation in curved steel plates and hollow steel cylinders", *Struct. Eng. Mech.*, **34**(3), 395-398.

Lu, Y., Ye, L., Wang, D., Zhou, L.M. and Cheng, L. (2010), "Piezo-activated Guided Wave propagation and interaction with damage in tubular structures", *Smart. Struct. Syst.*, **6**(7), 835-849.

Moilanen, P., Nicholson, P.H.F., Kilappa, V., Cheng, S. and Timonen, J. (2006), "Measuring guided waves in long bones: Modeling and experiments in free and immersed plates", *Ultrasound. Med. Biol.*, **32**(5), 709-719.

Moilanen, P., Talmant, M., Kilappa, V., Nicholson, P., Cheng, S. L., Timonen, J. and Laugier, P. (2008), "Modeling the impact of soft tissue on axial transmission measurements of ultrasonic guided waves in human radius", *J. Acoust. Soc. Am.*, **124**(4), 2364-2373.

Na, W.B. and Kundu, T. (2002), "Underwater pipeline inspection using guided waves", *J. Press. Vess - t. Asme.*, **124**(2), 196-200.

Protopappas, V.C., Fotiadis, D.I. and Malizos, K.N. (2006), "Guided ultrasound wave propagation in intact and healing long bones", *Ultrasound. Med. Biol.*, **32**(5), 693-708.

Su, Z. and Ye, L. (2009), *Identification of damage using lamb waves: From fundamentals to applications*, Springer-Verlag, Berlin Heidelberg.

Yapura, C.L. and Kinra, V.K. (1995), "Guided waves in a fluid-solid bilayer", *Wave Motion*, **21**(1), 35-46.

Yu, J.G. and Ma, Z.J. (2012), "Guided viscoelastic Wave in circumferential direction of orthotropic cylindrical curved plates", *Struct. Eng. Mech.*, **41**(5), 605-615.